JJMIE

Volume 19, Number 3, Sep. 2025
ISSN 1995-6665
Pages 641– 655
https://doi.org/10.59038/jjmie/190316
Editor-in-Chief: Prof. Ali M. Jawarneh

Jordan Journal of Mechanical and Industrial Engineering

Optimization of Performance and Economic Viability in Trans-critical CO_2 Air Conditioning Systems Incorporating Solar-Powered Mechanical Subcooling

Mohammad Tarawneh[1], Ahmad Bani Yaseen[1*], Lina AL-Zahrani[1], Hitham Tlilan[1]

[1]*Department of Mechanical Engineering,Faculty of Engineering, The Hashemite University, Zarqa, Jordan*

Received 1 Jun 2025 *Accepted 28 Jul 2025*

Abstract

This study investigates the thermodynamic performance and economic feasibility of a trans-critical CO_2 air conditioning system integrated with a solar-powered mechanical sub-cooler, developed to enhance cycle efficiency and reduce energy consumption under Jordan's climatic conditions. The system introduces a novel hybrid approach by incorporating R-423A as an environmentally friendly substitute for R-22, alongside a solar-assisted mechanical sub-cooling cycle. Unlike conventional approaches that assess sub-cooling or refrigerant replacement in isolation, this study examines the combined effect of both, under varying operational and environmental parameters. The influence of ambient temperature, gas cooler pressure, evaporation temperature, and sub-cooling degree on the system's combined coefficient of performance (COPcomb) is thoroughly analyzed. In addition, the effects of solar time and solar panel area on COP and compressor power consumption are evaluated. Results indicate a substantial improvement in system performance, with COP increasing by 70–75% when the sub-cooling temperature reaches 14°C. However, raising the sub-cooling temperature from 0 to 16°C at an ambient temperature of 35°C increases combined cycle power consumption by 25.7%. The system, equipped with a 6.4 m² solar panel, achieves a maximum utility power savings of 68.3%. An economic analysis demonstrates annual energy savings of 2,310 kWh, with a favorable payback period, affirming the system's financial viability. Overall, the integration of solar energy and mechanical sub-cooling offers a promising, sustainable solution for enhancing CO_2 system performance and reducing operating costs in hot climates.

Keywords: Trans-critical CO_2, Solar Energy, Sub-cooling, Air conditioning, Simulation.

1. Introduction

This research presents a novel integration of a solar-powered mechanical sub-cooling system at the gas cooler outlet of a 4-ton trans-critical CO_2 air conditioning unit, optimized for Jordan's high solar potential. With over 150 sunny days between May and October (Ministry of Energy and Mineral Resources (MEMR), Annual Reports, 2023) [25], Jordan offers ideal conditions for leveraging solar energy to enhance refrigeration efficiency. The study uniquely combines solar-assisted mechanical sub-cooling with the use of R-423A as a replacement for R-22, addressing both environmental impact and system performance.

A comprehensive simulation evaluates the system's behavior under Jordanian summer conditions, analyzing the effects on power consumption, cooling capacity, and overall COP. Unlike previous studies that treat refrigerant substitution or sub-cooling in isolation, this work explores their combined impact in a real-world climatic context. The analysis highlights substantial improvements in energy efficiency and operational performance, while demonstrating notable utility savings and reduced environmental footprint.

Economic feasibility is also assessed, showing that solar-assisted sub-cooling can lead to significant cost savings and a practical payback period, making it suitable for residential, commercial, and industrial applications. The study emphasizes the importance of adapting refrigeration systems to local climate conditions to maximize performance.

By bridging solar energy integration with high-pressure refrigeration technologies, this research offers a sustainable pathway for next-generation cooling systems. It builds on previous work while introducing a practical, location-specific solution marking a significant advancement in the field of energy-efficient, climate-adapted air conditioning.

Researchers increasingly focus on utilizing renewable energy for thermal and air conditioning applications, with the trans-critical carbon dioxide cycle gaining popularity in recent years. This cycle has undergone various improvements to enhance its performance over time. Over the years, researchers have investigated multiple techniques

* Corresponding author e-mail: ahmadi_ah@hu.edu.jo.

to enhance the efficiency of refrigeration and air conditioning systems. Dai et al. [1] explored R152a in a single-stage mechanical sub-cooling cycle, highlighting its advantages at low evaporation levels and high heat rejection temperatures. They optimized gas-cooler pressure and sub-cooling extent, later extending their analysis to zeotropic mixtures to further improve cycle performance. In a parallel effort, Nebot-Andrés et al. [2] compared a dedicated mechanical sub-cooling system with a cascade refrigeration system, concluding that the former offered higher energy efficiency, especially when evaporation exceeded -15°C and in warmer climates. Building on these findings, Catalán-Gil et al. [3] examined integrated and specialized mechanical sub-cooling cycles for supermarket boosters, identifying up to a 3.4% energy reduction in warm regions and 2.4% in hotter climates. Meanwhile, Llopis et al. [4] investigated a trans-critical cycle with mechanical sub-cooling using R290, demonstrating that dedicated sub-cooling enhanced the total coefficient of performance (COP) by approximately 18.4%. Expanding on CO_2 applications, Cao et al. [5] explored a hybrid CO_2 system for space heating, achieving a 15.3% COP gain compared to conventional CO_2 heat pumps. Bahman et al. [6] further advanced air conditioning systems by integrating vapor injection technology, which significantly improved performance, particularly in hot climates. The role of artificial intelligence in performance prediction was explored by Sencan et al. [7], who used artificial neural networks to assess the effects of sub-cooling and super-heating on refrigeration system COP. In a different direction, Zhang et al. [8] investigated a solar-powered trans-critical CO_2 cycle for combined electricity and heat generation, confirming efficiency improvements across summer and winter conditions. The concept of solar-assisted cooling was extended by Anas Farraj et al. [9], who examined hydrocarbon mixtures as replacements for R-22 in solar-powered air conditioners, reporting a 35% reduction in compressor power consumption using liquefied petroleum gas mixtures (LPGM).Recognizing Jordan's solar energy potential, Ali M. Jawarneh et al. [10] analysed energy availability, concluding that surfaces with a 45° slope provided maximum winter energy capture, while those with a 20° slope optimized summer energy absorption. Li et al. [11] investigated the relationship between cooling output and sub-cooling power, determining that adjusting sub-cooling power alone does not significantly boost cooling capacity. In contrast, Mehdi Zeyghami et al. [12] reviewed various solar thermo-mechanical cooling techniques, providing insights into system improvements. Sarbu and Sebarchievici [13] further categorized different solar refrigeration systems, comparing thermal and solar-electrically driven cooling methods.Several studies have emphasized the integration of solar powered into mechanical refrigeration systems. Bellos et al. [14] performed a performance simulation of a solar-assisted compression refrigeration system, demonstrating that the optimization of evaporation and condensation temperatures can lead to a significant improvement in the coefficient of performance (COP). Hanslik et al. [15] examined mechanical sub-cooling using water as a refrigerant in a trans-critical CO_2 cycle, achieving efficiency gains exceeding 35%. Similarly, Santosa et al. [16] conducted an analysis of trans-critical CO_2 refrigeration systems using Engineering Equation Solver (EES), verifying a progressive decline in the coefficient of performance (COP) with increasing ambient temperatures, while confirming the system's operational feasibility. Sara Barghash et al. [17] assessed a solar-assisted mechanical sub-cooling air conditioning system, reporting a COP improvement of 5% to 16% through EES simulations. Mohammad Tarawneh [18] optimized a porous gas cooler in a trans-critical CO_2 refrigeration cycle, reducing porosity and gas cooler outlet temperature by 34% and 36°C, respectively, leading to a remarkable 94.4% COP increase and an 85.5% improvement in heat rejection rates. Another study by Mohammad Tarawneh [19] investigated the influence of variation of porosity as well as outside air temperature and refrigerant evaporation temperature on the cycle coefficient of performance, evaporation capacity, pressure drop, and power consumption during the compression process.Expanding on refrigerant comparisons, Mohammad Tarawneh et al. [20] experimentally analysed the impact of super-heating temperature variations on three refrigerants (R-404A, R22, and R422A), demonstrating that R-422A and R-404A outperformed R-22, particularly in low-temperature applications. Rodrigo Llopis et al. [21] explored energy advantages of integrating mechanical sub-cooling with a CO_2 trans-critical refrigeration cycle, reporting a 55.7% increase in COP and a 30.3% rise in refrigeration capacity using R1234yf refrigerant.

Anes Guedour et al. [22] explored the integration of a solar-powered mechanical subcooling cycle into a conventional vapor compression system, focusing on hot climates like Kuwait. Their study included exergy, environmental, and economic analyses, revealing improved system efficiency, reduced environmental impact, and a payback period of about nine years. The results highlight the potential of solar-assisted subcooling to enhance performance and long-term cost-effectiveness in high-temperature regions.Mohammad Tarawneh et al. [23] presented a novel approach combining internal heat exchanger (IHEX) modifications with solar PV systems to enhance the coefficient of performance (COP) and reduce power consumption in Jordan’s climate. Their findings demonstrated significant performance improvements under optimized conditions. At an optimal gas cooler pressure of 9111 kPa, the IHEX contributed to a 45% increase in COP. Furthermore, increasing the gas cooler pressure from 8000 to 9111 kPa resulted in a 40% COP enhancement. Reducing the ambient temperature from 35 °C to 28 °C led to a substantial 73% improvement in system efficiency, highlighting the effectiveness of the proposed integration in hot climatic regions. Xiang Qin et al. [24] presented a comparative analysis of trans-critical CO_2 heat pump systems with and without ejector: performance, exergy, and economic perspective. Their experimental results revealed that the ejector-assisted mode not only achieves a higher water outlet temperature and reduces compressor power consumption but also improves the system’s exergy efficiency by 6.6% under the condition of the maximum outlet water temperature.

Although solar-assisted cooling and trans-critical CO_2 systems have been widely studied, there is limited research on integrating solar-powered mechanical sub-cooling with trans-critical CO_2 cycles under extreme climates. This study

addresses that gap by evaluating the techno-economic performance of a 4-ton CO_2 air conditioning system enhanced with a solar-powered mechanical sub-cooler in Jordan's hot climate. Unlike previous studies that focused on either refrigerant replacement or sub-cooling alone, this work uniquely investigates the combined effects of R-423A as an R-22 substitute and solar-assisted sub-cooling. It is the first to analyse the influence of ambient temperature on this integrated setup while assessing both energy performance and cost-effectiveness, offering a novel and sustainable solution for air conditioning in high-temperature regions. A comparative evaluation with other enhancement methods will be considered in future work**.**

2. Operational Cycle Description

Figure 1 illustrates the schematic diagram of the solar-powered mechanical sub-cooler air-conditioning system. The system consists of a 4-ton trans-critical CO_2 air conditioning unit, including an evaporator, compressor, gas cooler, and expansion valve, integrated with a mechanical sub-cooling cycle powered by solar photovoltaic (PV) cells. The lower section of the diagram represents the base trans-critical CO_2 cycle, while the upper section depicts the solar-assisted mechanical sub-cooling cycle utilizing R423A as the refrigerant. The thermophysical properties of CO_2 and R423A are listed in Table I.

Figure 2 illustrates the pressure-enthalpy diagram of the trans-critical CO2 cycle. The cycle begins as trans-critical CO2 flows through the gas cooler at constant pressure (process 2-3), where it rejects heat to the surroundings. After leaving the gas cooler, the refrigerant remains in a superheated state at point 3.

To enhance cooling performance, the superheated CO2 undergoes additional sub-cooling through the mechanical sub-cooler (process 3-4), where heat is extracted and transferred to the sub-cycle evaporator (process 10-7) in the upper section of the combined cycle, as shown in Figure 1.

Following sub-cooling, CO2 is expanded through an expansion valve (process 4-5), causing a sudden drop in pressure and temperature, leading to a liquid-vapor mixture at state 5. This mixture then enters the evaporator (process 5-6), where it absorbs heat from the surroundings, transitioning into a saturated vapor at state 6.

The saturated vapor then undergoes superheating (process 6-1), ensuring it remains in the vapor phase before entering the compressor at state 1. This step prevents liquid refrigerant from entering the compressor, which could cause mechanical damage. The cycle then repeats, maintaining efficient refrigeration operation.

Figure 3 displays the pressure-enthalpydiagram for the mechanical sub-cooling cycle. It is assumed that the condensation and evaporation processes took place without a pressure drop at constant temperatures and pressures.

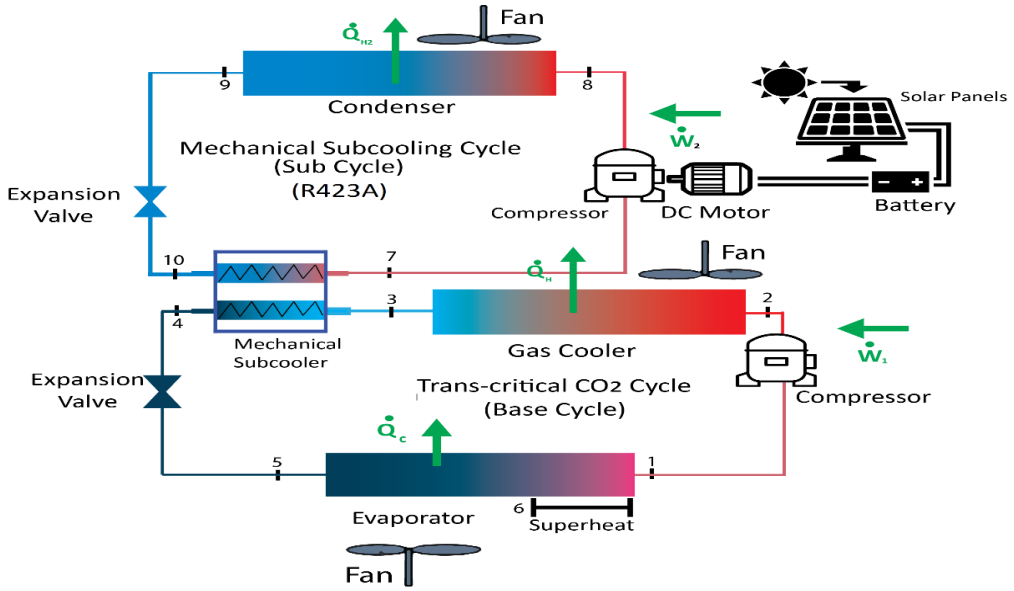

Figure 1. Schematic representation of the air conditioning system

Table I. Thermophysical properties of CO_2, R423A, and R1234yf. Kim et al. [26]

Refrigerant	ODP	GWP	P_{cr} kPa	Latent heat of vaporization at -26.1°C (kJ/kg)	Density Kg/m^3 (at 20C° and 100kPa)	Boiling point (at 100kPa)	Critical temperature °C
CO_2(R-744)	0	1	7380	294	1.839	194.6	31
R423A	0	2280	3550	160	1279	-24.1	100
R1234yf	0	4	3330	146	1097	-29.5	94.7

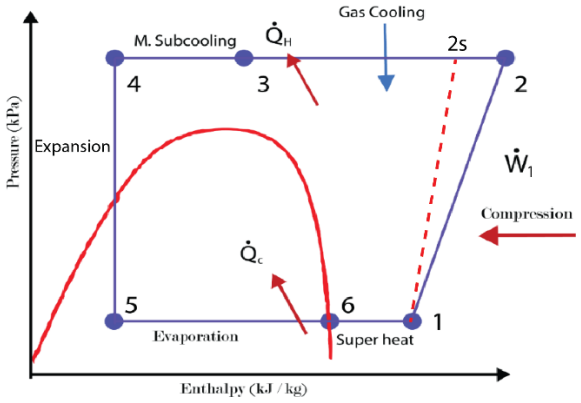

Figure 2. Pressure-enthalpy diagram of the trans-critical CO_2 cycle.

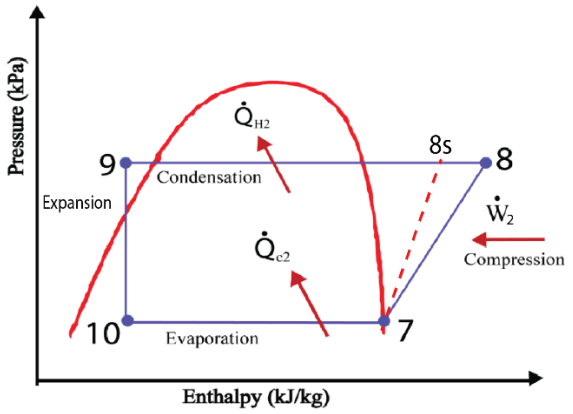

Figure 3. Pressure-enthalpy diagram for the mechanical sub-cooling cycle.

3. ModelingAssumptions

The fundamental assumptions taken into account during this simulation investigation are summarized in the following points:

- The system operates under steady-state conditions, with transient effects neglected.
- Thermophysical properties of CO_2 are sourced from the EES database.
- Pressure losses in pipes and thermal components are considered negligible.
- Gas cooler and evaporator efficiencies are assumed constant, based on standard performance metrics.
- All components (e.g., compressor, heat exchangers) are assumed to function without significant heat losses to the environment.
- Ambient temperature is considered constant during each simulation run to ensure uniform boundary conditions.
- The solar photovoltaic system is assumed to provide sufficient and reliable power under optimal solar conditions.
- Solar irradiance is assumed to average 5.5 kWh/m²/day, reflecting high solar potential in regions such as Jordan.

4. Solar Energy Availability and PV Analysis

Solar energy is considered one of the most favorable alternative energy sources owing to its low environmental impact, economical nature, easy deployment, and modest system requirements. Jordan possesses significant potential for solar energy utilization due to its location within the global solar belt, where average solar irradiance ranges between 5 and 7 kWh/m², which suggests a capacity of at least 1000 GWh yearly (Ministry of Energy and Mineral Resources (MEMR), Annual Reports, 2023) [25]. As a result, it is desirable to use the solar energy that is currently accessible in this study to attain higher efficiency.

The following mathematical formula is utilized to estimate the solar PV power[17]:

$$\dot{W}_{(solar)} = \eta_{PV} \times I \times A \times \alpha \quad (1)$$

Where A is the area (m^2) of the solar panels, which will be chosen based on the criteria explicitly listed in the section below,(I) is the total irradiance (W/m^2), (α) is the absorptivity of the surface, and (η_{PV}) is the efficiency of the PVs, which is calculated using equation 2 [17]:

$$\eta_{PV} = 0.553 - 0.001T_{PV} \quad (2)$$

Where T_{PV} is the temperature (K) of the solar panel,whichis calculated as per equation3[27]:

$$T_{PV} = T_{amb} + I \times e^{(-3.473-0.0594\times V_w)} \quad (3)$$

T_{amb} stands for the outside temperature (°C), and V_w for the wind speed (m/s). In Jordan, average daily solar irradiance and ambient temperatures have been measured.

5. Modeling of The Thermodynamic Cycles

The base trans-critical air conditioning cycle with and without sub-cooling is modeled by using the thermodynamics laws. The subscripts used in the equations correspond to the state points indicated in**Figures** 1, 2, and 3, observing that there will only be four states if the base cycle is present. State 4 in **Figure 2** will not be taken into account; instead, state 5 will be regarded as the fourth state. According to Klein and Alvarado [28], an engineering equation solver program called EES is used to resolve the modeled equations. EES is also utilized to carry out parametric analyses and obtain the refrigerant properties. Equations 4 and 5 definethe compressor power consumption of the trans-critical base cycle and the enthalpy of CO_2 at the outlet of the compression process in the base cycle (h_2) , respectively, as follows:

$$\dot{W}_1 = \dot{m}_{base}(h_2 - h_1) \quad (4)$$

$$h_2 = \frac{h_{2s}-h_1}{\eta_{Comp1}} + h_1 \quad (5)$$

Where h_1 is the enthalpy of carbon dioxide at the input of the compressor in the base cycle (kJ/kg),$h_{2s}$is the enthalpy (kJ/kg)at the outlet of the isentropic compression process, $\dot{m}_{base}$is the mass flow rate of the refrigerant in the base cycle(kg/s) which is calculated based on the nominal capacity of the base cycle (14 kW) and η_{Comp1} is efficiency of the compressor of the base cycle, which can be calculated as per equation 6 [29]:

$$\eta_{comp1} = 1.003 - 0.12\ Pr1 \quad (6)$$

Where, Pr1 is the pressure ratio through the compressor of the base cycle, which can be found as per the equation7:

$$Pr1 = \frac{P2}{P1} \quad (7)$$

Where $P1$ and $P2$ are the pressures (kPa) at the inlet and outlet of the compression process in the base cycle, respectively.

Equation 8 can be used to determine the COP of the basecycle:

$$COP_{base} = \frac{h_1 - h_5}{h_2 - h_1} \quad (8)$$

Where h_5 is the enthalpy of CO_2(kJ/kg) at the evaporator input.

Equation 9 can be used to determine the varying cooling capacity of the base cycle (kW):

$$\dot{Q}_c = \dot{m}_{base}(h_1 - h_5) \quad (9)$$

Equation 10 is used to determine the mass flow rate (kg/s) of refrigerant in the mechanical sub-cooling cycle:

$$\dot{m}_{sub} = \dot{m}_{base}\left(\frac{h_3 - h_4}{h_7 - h_{10}}\right) \quad (10)$$

Where h_4, h_7 and $h_{10}$are the enthalpies (kJ/kg) at the mechanical sub-cooler outlet. Equation11 is used to calculate the power usage of the solar-powered compressor (kW):

$$\dot{W}_2 = \dot{m}_{sub}(h_8 - h_7) \quad (11)$$

Where $h_8$is the enthalpy (kJ/kg)at the compressor's outlet, it can be calculated as per equation 12:

$$h_8 = \frac{h_{8s} - h_7}{\eta_{Comp2}} + h_7 \quad (12)$$

Where h_{8s} is the enthalpy (kJ/kg) at the outlet of the isentropic compression process in the subcooling cycle,$\eta_{Comp2}$is the compressor efficiency in the subcooling cycle. which can be calculated as per equation 13 [29]:

$$\eta_{comp2} = 1.003 - 0.12\ Pr2 \quad (13)$$

Where Pr2 is the pressure ratio of the compressor of the subcooling cycle, which can be found as per equation 14:

$$Pr2 = \frac{P8}{P7} \quad (14)$$

Where $P7$ and $P8$ are the pressure (kPa) at the inlet and outlet of the compression process in the subcooling cycle,

Equation 15 is used to determine the combined cycle'stotal compressor power consumption (kW):

$$\dot{W}_{\text{comb}} = \dot{W}_1 + \dot{W}_2 \quad (15)$$

The coefficient of performance of the combined cycles is calculated by Equation 16:

$$COP_{comb} = \frac{\dot{Q}_c}{\dot{W}_{\text{comb}}} \quad (16)$$

Then, using equation 17, it is crucial to assess the enhancement in COP value (COP_{enh}) by contrasting the COP of the combined cycle with that of the base cycle with no sub-cooling:

$$COP_{enh}\% = \frac{\text{COP}_{\text{comb}} - \text{COP}_{\text{base}}}{\text{COP}_{\text{base}}} \times 100 \quad (17)$$

Where$\text{COP}_{\text{base}}$is the base cycle's coefficient of performance without subcooling.

Equation18 is used to calculate the percentage increase in combined cycle power consumption.

$$\dot{W}_{comb,in}\% = \frac{\dot{W}_{\text{comb}} - \dot{W}_{\text{base}}}{\dot{W}_{\text{base}}} \times 100 \quad (18)$$

The study focused on a set of parameters known to significantly influence the cycle's efficiency and overall performance. **Table II** contains a list of operating simulation parametersand boundary conditions.

Table II. Operation simulation parameters and boundary conditions

Parameters	Range value	Constant value
Gas cooler pressure (P_{gc})	8500 – 15500 kPa	10000 kPa
Gas cooler outlet temperature	35 – 50°C	45 °C
Evaporation temperature (T_{evap})	10 – 20 °C	16 °C
Ambient temperature (T_{amb})	30 – 45 °C	30 °C
Trans-critical cycle compressor efficiency	Equation 6	0.8
Subcooling cycle compressor efficiency	Equation 13	0.8
Degree of sub-cooling (ΔT_{sub})	0 –16 °C	4 °C and 16°C
Degree of super-heat (ΔT_{sup})	0 –16 °C	0 °C

Referring to Figures 1,2, and 3, Table III presents the modeling equations for the thermodynamic properties at each state point of the cycles. The refrigerant properties x and s that appear in Table III refer to the quality (%) and the entropy(kJ/K), respectively, also the refrigerant properties, s_{2s} and s_{8s} referto the entropies(kJ/K) at the outlet of isentropic compression processes in the trans-critical base cycle and the sub-cooling cycle, respectively. The EES software utilizes thermodynamic equations and the thermal properties of refrigerants to solve the model. Figure 4 presents the flowchart of the modeled system.

Table III. Thermodynamic property modeling equations for each state point of the cycles.

State 1	State 2	State 3	State 4	State 5
$T_1=T_6+T_{sup}$ $P_1=P_6$ $h_1=h\ (T_1, P_1)$ $s_1=s(T_1,P_1)$	$s_{2s}=s_1$, $P_2=P_{gc}$ $h_{2s}=h(s_{2s}, P_2)$ $h_2=h_1+(h_2-h_1)/\eta_{c,1}$ $s_2=s(h_2,P_2)$ $T_2=T(s_2,P_2)$	$T_3=T_{gco}$ $P_3=P_2$ $h_3=h(T_3,P_3)$ $s_3=s(T_3,P_3)$	$T_4=T_3+T_{sub}$ $P_4=P_3$ $h_4=h(T_4,P_4)$ $s_4=S(T_4,T_4)$	$h_5=h_4$ $P_5=P_6$ $T_5=T_6$ $x_5=x(T_5,h_5)$ $s_5=s(T_5,h_5)$
State 6	**State 7**	**State 8**	**State 9**	**State 10**
$T_6=T_{evap}$ $x_6=$ *sat vapor* $P_6=P(T_{evap},x_6)$ $h_6=h(P_6,x_6)$ $s_6=s(P_6,x_6)$	$P_7=P_{10}$ $x_7=$ *sat vapor* $T_7=T_{10}$ $h_7=h(P_7,x_7)$ $s_7=s(P_7,x_7)$	$s_{8s}=s_7$ $P_8=P_9$ $h_{8s}=h(s_{8s},P_8)$ $h_8=h_7+(h_8-h_7)/\eta_{c,2}$ $s_8=s(h_8,P_8)$ $T_8=T_9$	$T_9=T_{cond}$ $x_9=$ *sat liquid* $P_9=P(T_{cond},x_9)$ $h_9=h(P_9,x_9)$ $s_9=s(P_9,x_9)$	$T_{10}=T_9-T_{HX}$ $h_{10}=h_9$ $P_{10}=P(T_{10},h_{10})$ $s_{10}=s(T_{10},h_{10})$

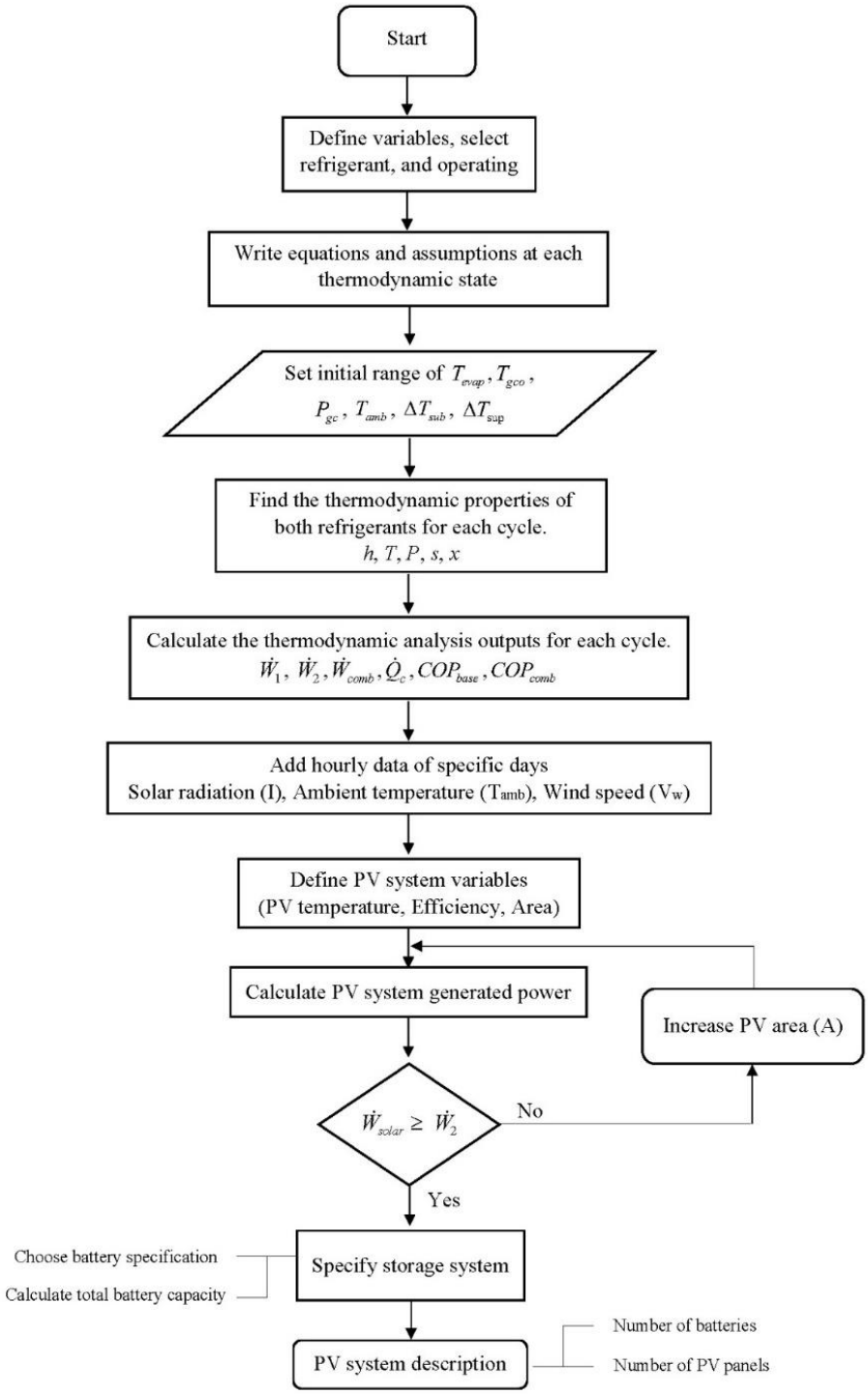

Figure 4. The modeling system flow chart.

6. Model validation

The simulation model in this study has been validated using experimental data from Llopis et al. [21], who investigated the energy performance of a CO_2 trans-critical refrigeration system integrated with a mechanical subcooling cycle. The experimental setup involved a single-stage CO_2 trans-critical refrigeration plant combined with a semi-hermetic compressor operating with an R1234yf subcooling cycle. The system was tested at heat rejection temperatures of 24°C, 30°C, and 40°C, with two different CO_2 cycle evaporation levels (0°C and -10°C).For validation, the experimental work was conducted under the following conditions: a dedicated mechanical subcooling system using R1234yf as the working fluid, a superheat temperature difference (ΔT_{sup}) of 5°C, a subcooling temperature difference (ΔT_{sub}) of 5°C, an evaporation temperature (T_{evap}) of 0°C, a gas cooler outlet temperature (T_{gco}) of 41.7°C, a compressor efficiency of 0.6, and a CO_2 mass flow rate of 0.0667 kg/s.

The combined coefficient of performance (COP_{comb}) from the experimental study was compared with the simulated results from this study. **Figure 5** represents the experimental and the simulated approaches of the variation of COP_{comb} with gas cooler pressure (P_{gc}). The figure shows that both the experimental and simulated results exhibit similar trends. The average percentage deviation between the experimental and simulated COP_{comb} values was found to be 7.9%. This deviation is attributed to slight differences in assumed system efficiencies, refrigerant properties, and heat transfer coefficients in the simulation model compared to real-world experimental conditions.Similarly, the refrigeration capacity ($\dot{Q}c$) of the CO_2 trans-critical cycle was validated against the experimental data. **Figure 6** presents the variation of refrigeration capacity with P_{gc} for both the simulated and experimental approaches. The comparison confirms that the simulation model follows the experimental trends closely, with an average percentage deviation of 4.35%. The deviation can be explained by minor discrepancies in compressor modeling, heat exchanger performance, and ambient conditions. Overall, the validation results confirm that the developed simulation model provides a reliable representation of the experimental system. The relatively low deviations indicate that the model can effectively predict the performance of a solar-powered mechanical subcooling system under varying operating conditions. It is acknowledged that the experimental data used for validation involved R1234yf in the subcooling cycle rather than R423A. However, the validation focused on capturing system behavior and performance trends, such as COP and cooling capacity variations with gas cooler pressure, which remain consistent across similar low-pressure refrigerants. R1234yf and R423A exhibit comparable thermodynamic characteristics in subcooling applications, justifying the use of the available data. Furthermore, R423A-specific properties were accurately applied in the simulation model to ensure realistic system predictions. This approach provides a reasonable and practical basis for validating the simulation under the current data limitations. Nonetheless, to strengthen the findings and address refrigerant-specific effects, future work will include experimental validation using R423A in the subcooling cycle.

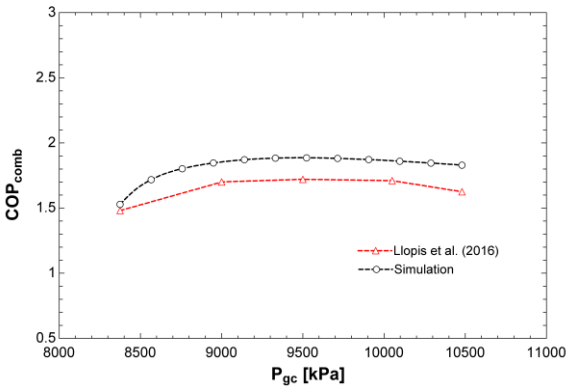

Figure 5. Variation of COP_{comb} with $P_{gc}$for the experimental and the simulated approaches

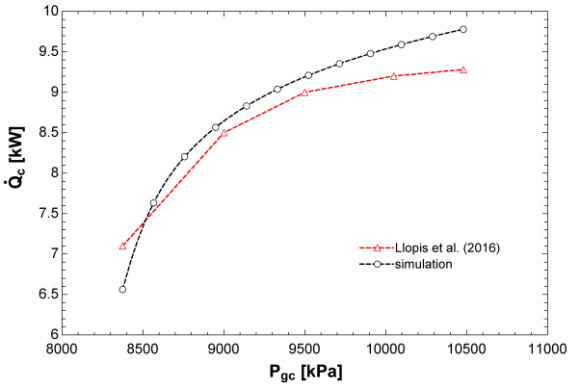

Figure 6. Variation of $\dot{Q}_c$with P_{gc} for the experimental and simulated approaches.

7. Results and Discussions

7.1. Effect of degree of subcooling on the performance of air conditioning cycle.

All of the above computations involved in this simulation analysis are made by Engineering Equation Solver (EES) by using its in-built thermodynamic and heat transfer property functions. Moreover, the in-built properties facilitate the incorporation of a solar system (PV) in the sub-cooling cycle for power generation.

Figure 7 shows the variation of combined coefficient of performance (COP_{comb}) with sub-cooling temperature difference (ΔT_{sub}) at different ambient temperatures (T_{amb}), under the following conditions: T_{evap} = 16°C, T_{gco} = 45°C, P_{gc} = 10,000 kPa, ΔT_{sup} = 0°C, and compressor efficiency η_{comp} = 0.8. As ΔT_{sub} increases, the refrigerant exits the mechanical sub-cooler at a lower temperature, increasing the enthalpy difference across the evaporator and improving COP_{comb} due to a higher refrigeration effect. COP_{comb} also rises as T_{amb} decreases, since lower ambient temperatures enhance heat rejection in the gas cooler, reducing refrigerant temperature before expansion. Results show that reducing T_{amb} leads to an average COP_{comb} increase of 40.7%. At T_{amb} = 35°C, increasing ΔT_{sub} from 2°C to 15°C boosts COP_{comb} by approximately 18.8%. These findings confirm that both higher sub-cooling and lower ambient temperatures significantly enhance system efficiency. Mechanical subcooling, therefore, plays a key role in improving the performance of trans-critical CO_2 systems under varying climatic conditions.

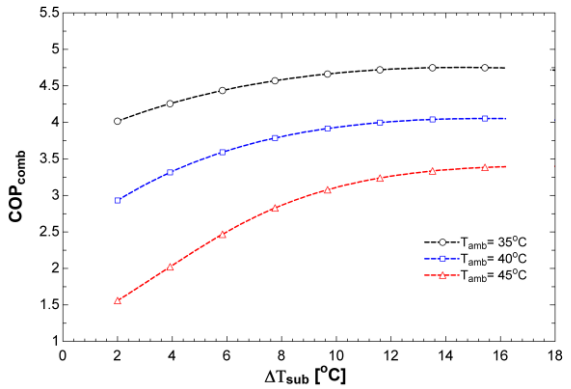

Figure 7. Variations of $COP_{comb}$with ΔT_{sub} for different values of T_{amb}

Figure 8 shows how the combined coefficient of performance (COP_{comb}) varies with gas cooler outlet temperature (T_{gco}) for different subcooling temperature differences (ΔT_{sub}) = 0–16°C), under the conditions: T_{evap} = 16°C, P_{gc} = 10,000 kPa, ΔT_{sup} = 0°C, and η_{comp} = 0.8. COP_{comb} decreases as T_{gco} increases due to a higher-pressure ratio, which raises compressor work and lowers the refrigeration effect. At ΔT_{sub} = 0°C, COP_{comb} drops by 77.8% with rising T_{gco}, and by 57.2% at ΔT_{sub} = 16°C. Conversely, increasing ΔT_{sub} improves COP_{comb}, with a ~70.83% gain observed at T_{gco} = 45°C when ΔT_{sub} rises from 0°C to 16°C. These results highlight the significant efficiency losses from high T_{gco} and the mitigating benefits of mechanical subcooling, which enhances system performance under elevated gas cooler temperatures.

Figure 9 shows the variation of COP_{comb} with gas cooler pressure for different subcooling levels (ΔT_{sub} = 0 –16°C), under the conditions: T_{evap} = 16°C, T_{gco} = 45°C, ΔT_{sup} = 0°C, and η_{comp} = 0.8. COP_{comb} initially increases with P_{gc} due to improved heat rejection and enhanced refrigeration effect. However, beyond P_{gc} = 11,000 kPa, further increases reduce COP_{comb} as compressor work rises faster than the cooling gain. The impact of P_{gc} varies with ΔT_{sub}: at ΔT_{sub}= 4°C, COP_{comb} increases by 148%, while at ΔT_{sub}= 16°C, the gain is just ~5%, indicating diminishing returns at higher subcooling. Additionally, at P_{gc} = 11,000 kPa, increasing ΔT_{sub} from 0°C to 16°C raises COP_{comb} by 70.8%, confirming the strong efficiency boost from mechanical subcooling. In summary, while COP_{comb} peaks at optimal P_{gc} = 11,000 kPa, mechanical subcooling consistently enhances performance across all pressure levels, making it vital for trans-critical CO_2 system optimization.

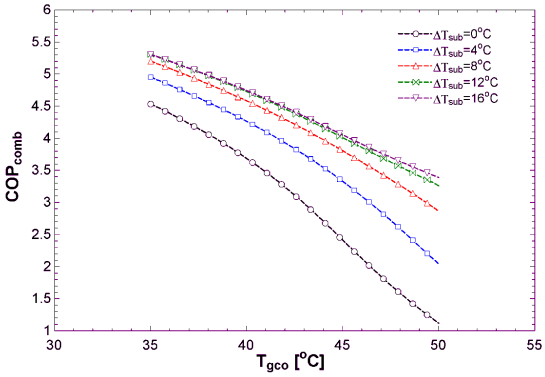

Figure 8. Variations of COP_{comb} with T_{gco} for different values of ΔT_{sub}

Figure 10 shows the variation of combined power consumption ($\dot{W}_{comb}$) with gas cooler pressure for subcooling levels (ΔT_{sub}) from 0°C to 16°C, under T_{evap} = 16°C, T_{gco} = 45°C, ΔT_{sup} = 0°C, and η_{comp} = 0.8. $\dot{W}_{comb}$ increases with both P_{gc} and ΔT_{sub}. Higher P_{gc}raises the pressure ratio, boosting compressor power, while higher ΔT_{sub} improves cooling but adds load. At ΔT_{sub} = 4°C, $\dot{W}_{comb}$ increases by 133%, compared to 56% at 16°C. For P_{gc} = 11,000 kPa, increasing ΔT_{sub} from 0°C to 16°C raises $\dot{W}_{comb}$ by 17.4%. Similarly, raising P_{gc} from 8,500 to 11,000 kPa at ΔT_{sub} = 4°C results in a 56.7% increase. Thus, while subcooling boosts performance, it also elevates power demand, highlighting the need for an efficiency–consumption trade-off in trans-critical CO_2 systems.

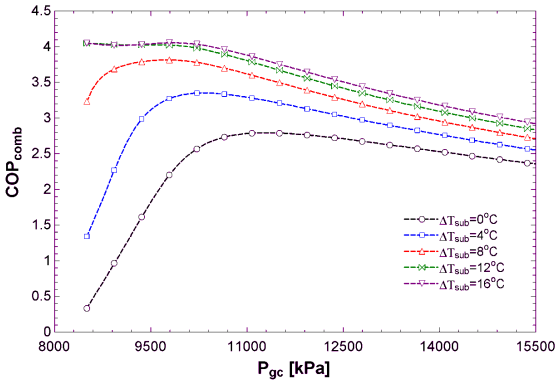

Figure 9. Variation of COP_{comb} with P_{gc} for different values of ΔT_{sub}

Figure 11 illustrates how COP_{comb} varies with evaporation temperature (T_{evap}) for subcooling levels (ΔT_{sub}) from 0°C to 16°C, under T_{gco} = 45°C, P_{gc} = 10,000 kPa, ΔT_{sup} = 0°C, and η_{comp}= 0.8. COP_{comb} increases with both T_{evap} and ΔT_{sub}. Higher T_{evap} lowers the compressor pressure ratio, reducing power use and boosting efficiency, while greater ΔT_{sub}enhances cooling capacity. At ΔT_{sub}= 0°C, COP_{comb} rises by 35%, and by 28.6% at ΔT_{sub}= 16°C. At T_{evap} = 15°C, increasing $\Delta T_{sub}$from 0°C to 16°C raises COP_{comb} by 69.6%. Also, raising T_{evap} from 10°C to 20°C at ΔT_{sub}= 16°C improves COP_{comb} by 28.6%. Conversely, low T_{evap} or ΔT_{sub} reduces efficiency due to higher compressor work and lower cooling effect. Overall, both parameters are critical for optimizing trans-critical CO_2 system performance.

Figure 12 shows how combined power consumption varies with evaporation temperature (T_{evap}) for subcooling levels from 0°C to 16°C, under T_{gco} = 45°C, P_{gc} = 10,000 kPa, ΔT_{sup} = 0°C, and η_{comp} = 0.8. $\dot{W}_{comb}$ decreases as T_{evap} increases, due to a lower compressor pressure ratio. At ΔT_{sub}= 0°C, $\dot{W}_{comb}$ drops by 39.2%, and by 32.3% at ΔT_{sub}= 16°C. Raising T_{evap} from 10°C to 20°C at ΔT_{sub}= 16°C reduces $\dot{W}_{comb}$ by 45.9%. In contrast, increasing ΔT_{sub} raises $\dot{W}_{comb}$, as enhanced cooling performance requires more compressor input. Thus, optimizing both T_{evap} and $\Delta T_{sub}$is essential to balance energy consumption and system efficiency in trans-critical CO_2 applications.

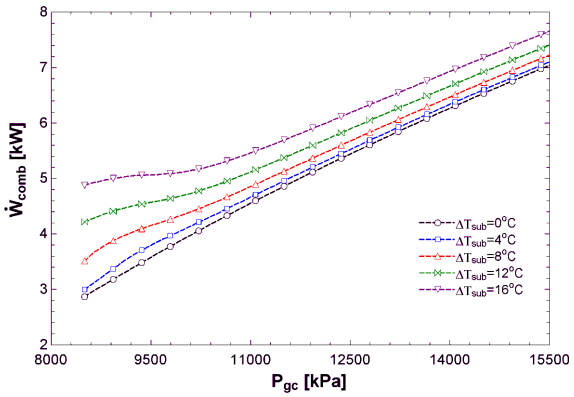

Figure 10. Variation of $\dot{W}_{comb}$ with P_{gc} for different values of ΔT_{sub}

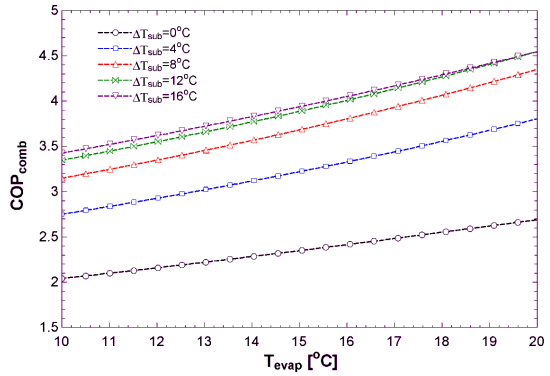

Figure 11. Variation of $COP_{comb}$with T_{evap} for different values of ΔT_{sub}.

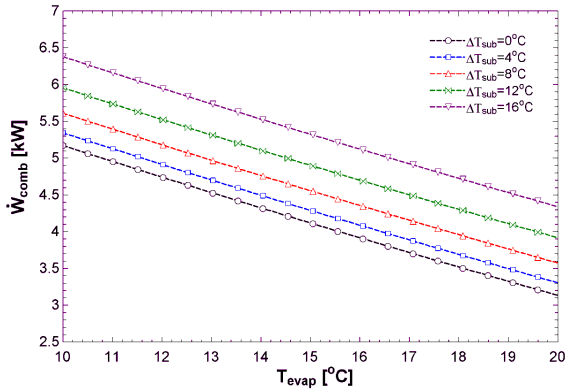

Figure 12. Variations of $\dot{W}_{comb}$ with T_{evap} for different values of ΔT_{sub}

Figure 13 shows the variation of COP_{comb} with ambient temperature (T_{amb}) for subcooling levels from 0°C to 16°C, under T_{evap} = 16°C, T_{gco} = 45°C, P_{gc} = 10,000 kPa, and η_{comp}= 0.8. COP_{comb} decreases as T_{amb}rises due to reduced heat rejection and increased compressor load. Conversely, increasing ΔT_{sub}improves $COP_{comb}$by enhancing cooling efficiency. At T_{amb}= 30°C, raising $\Delta T_{sub}$from 0°C to 16°C increases $COP_{comb}$by 22.2%, and by 192.3% at T_{amb}= 45°C. Additionally, lowering $T_{amb}$from 45°C to 30°C, at ΔT_{sub}= 16°C boosts $COP_{comb}$by 55.9%. These results highlight the importance of optimizing both ambient conditions and subcooling to maximize trans-critical CO_2 system efficiency.

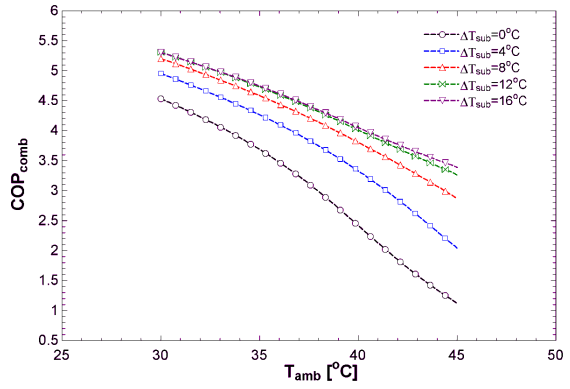

Figure13. Variations of COP_{comb} of R423a with T_{amb} for different ΔT_{sub}

Figure 14 illustrates the variation of combined power consumption with $T_{amb}$for subcooling levels from 0°C to 16°C, under T_{evap} = 16°C, T_{gco} = 45°C, P_{gc} = 10,000 kPa, and η_{comp} = 0.8. $\dot{W}_{(comb)}$ increases with T_{amb} due to reduced heat rejection and higher compressor workload. It also rises with ΔT_{sub}, as greater subcooling improves cooling but adds to compressor demand. At ΔT_{sub} = 8°C and 16°C, $\dot{W}_{(comb)}$ increases by 4.8% and 16.1%, respectively. At T_{amb}= 35°C, increasing ΔT_{sub} from 0°C to 16°C raises power consumption by 25.7%. Thus, while subcooling enhances performance, it also raises energy use, emphasizing the need to balance ΔT_{sub} and ambient conditions for optimal system efficiency.

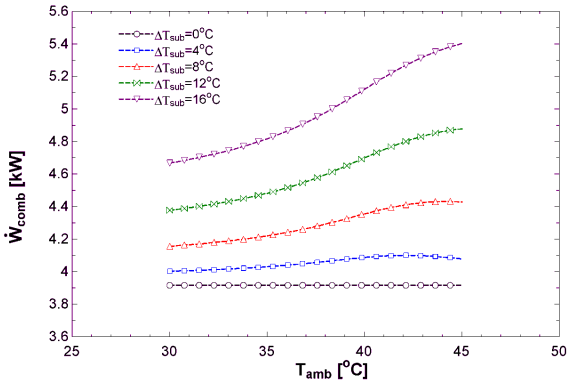

Figure 14. Variation of $\dot{W}_{comb}$ with T_{amb} for different ΔT_{sub}

Figure 15 shows the percentage increase in compressor power ($\dot{W}_{comb,in}$ %) versus $\Delta T_{sub}$and ΔT_{sup}, under T_{evap} = 16°C, T_{gco} = 45°C, $P_{(gc)}$ = 10,000 kPa, and $\eta_{comp_1} = \eta_{comp_2}$ = 80%. As ΔT_{sub} increases, $\dot{W}_{comb,in}$ %rises across all ΔT_{sup}levels due to increased refrigerant mass flow from denser liquid at the expansion valve. Similarly, higher ΔT_{sup}raises refrigerant enthalpy at the compressor inlet, increasing volumetric flow and compression work. At ΔT_{sub}= 14°C, $\dot{W}_{comb,in}$ % rises by 70–80% compared to ΔT_{sub}= 0°C, with a sharper increase beyond 10°C. Raising $\Delta T_{sup}$from 0°C to 16°C adds 25–35% to compressor power at any ΔT_{sub}. The widening gap between curves at higher ΔT_{sub} shows that superheat effects intensify with more subcooling. This underscores the need to balance both parameters for efficient compressor operation.

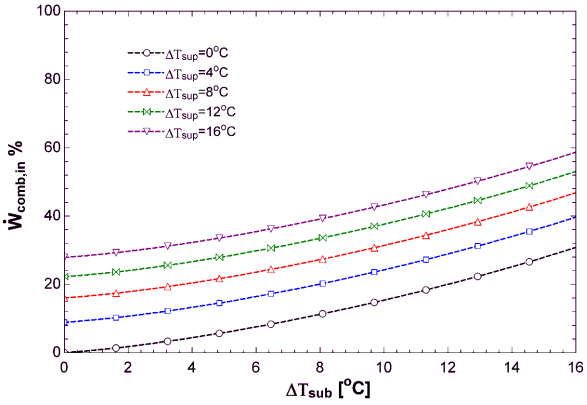

Figure 15. The percentage increase in combined cycle power consumptionas a function of (ΔT_{sub})

Figure 16 shows the COP enhancement (COP_{enh}%) versus ΔT_{sub} and ΔT_{sup}, under T_{evap} = 16°C, T_{gco}= 45°C, P_{gc} = 10,000 kPa, and $\eta_{comp_1} = \eta_{comp_2}$ = 80%. COP increases significantly with ΔT_{sub}, peaking at a 70–75% enhancement around 14°C due to improved refrigerating effect with nearly constant compressor work. Beyond 14°C, COP gain

slows, declining by 30%, as thermodynamic returns diminish and system complexity may rise. ΔT_{sup} also improves COP, but less effectively. Although it increases refrigerant enthalpy, it also raises inlet specific volume and compressor work, reducing net efficiency gains. At high ΔT_{sub}, the influence of ΔT_{sup}weakens, with COP curves converging. Thus, while both parameters enhance performance, subcooling is more impactful, and their combined optimization is essential for maximizing system efficiency.

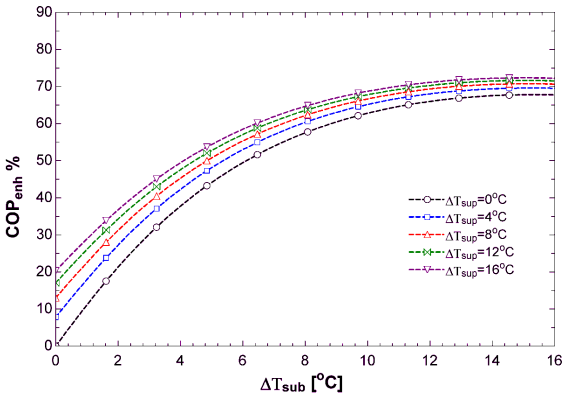

Figure 16. The percentage enhancement in COP of the combined refrigeration cycleas a function of ΔT_{sub}

A comparison of **Figures 15 and 16** reveals a critical trade-off: while increasing subcooling ΔT_{sub} boosts COP up to 75% at 14°C, it also raises compressor power by 70–80%, potentially offsetting efficiency gains. Additionally, the COP improvement rate drops by 30% beyond 14°C, indicating diminishing returns. Excessive subcooling also adds system complexity, larger heat exchangers, and higher refrigerant flow. Therefore, optimizing $\Delta T_{sub}$is essential to balance COP gains with compressor power and system practicality for efficient trans-critical CO_2 operation.

It is important to note that while subcooling significantly enhances the system's combined coefficient of performance (COP_{comb}), it also leads to an increase in power consumption due to the higher refrigerant mass flow rate and compressor workload. This dual effect is not contradictory but represents a common thermodynamic trade-off in trans-critical CO_2 systems. As demonstrated in **Figure 16**, COP_{comb} increases by up to 75% at a subcooling level of 14 °C, while **Figure 15** shows that compressor power consumption can rise by 70–80% at the same subcooling level. These findings indicate that although subcooling improves system efficiency, the associated power demand must be carefully managed to avoid diminishing returns. Therefore, optimizing the subcooling degree is essential to balance performance gains with energy input, particularly under varying ambient conditions. This highlights the practical need for system-level optimization in designing high-efficiency trans-critical CO_2 cycles.

7.2. Solar energy analysis

Jordan's climate is primarily sub-tropical arid, with clear skies and daily maximum temperatures exceeding 27°C from May to September. July is the hottest month, with an average high of 31°C. To assess PV module performance, five representative summer dates were selected: May 15, June 11, July 17, August 16, and September 15. Data were collected hourly in Zarqa, Jordan, using the Hashemite University solar station, including solar irradiance, sunshine hours, ambient temperature, and radiation intensity. As shown in **Figure 17**, solar irradiance peaked in mid-July and was lowest on September 15. In this study, the sub-cooling cycle compressor is powered by solar panels, which charge battery storage to enable 24-hour operation. The solar panel area was sized to meet the total energy demand of the sub-cooling cycle while ensuring continuous battery support.

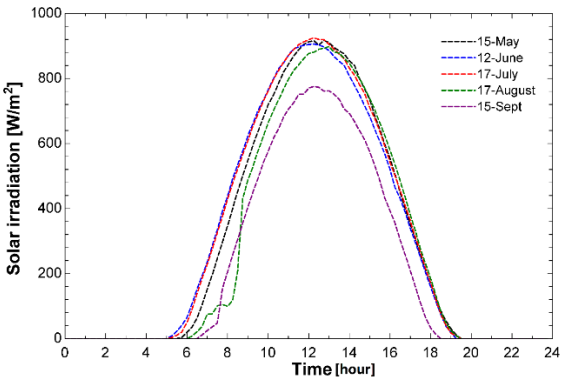

Figure 17. Solar irradiation for the average days of summer months.

Figure 18 presents the mechanical sub-cooling compressor power consumption ($\dot{W}_2$) throughout the day across selected summer months. Power consumption rises during daylight hours, peaking in the afternoon due to elevated ambient temperatures (T_{amb}), which increase the cooling load. As T_{amb} rises, the compressor requires more energy to maintain sub-cooling, leading to higher $\dot{W}_2$. At night, cooler ambient conditions reduce the load, lowering energy consumption. Among the months, August shows the highest $\dot{W}_2$, consistent with its typically higher average temperatures compared to May, June, July, and September. The daily power curve follows a typical trend: increasing in the morning due to residual thermal load and solar heat gain, peaking midday, then decreasing in the evening. This pattern aligns with ambient temperature and solar radiation variation. These results confirm the strong dependency of compressor energy use on ambient conditions, underscoring the need for optimized cooling strategies in hot climates like Jordan to enhance energy efficiency.

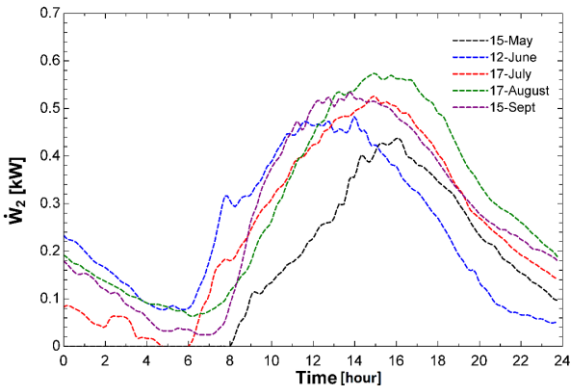

Figure 18. The compressor power consumption in the mechanical subcooling cycle as a function of time across representative average days of the summer months.

Figure 19 shows the daily variation of solar power generation ($\dot{W}_{solar}$) and compressor power consumption ($\dot{W}_2$) across different months, highlighting clear seasonal and diurnal trends. Solar power peaks in May due to longer daylight and stronger sunlight, while September records the lowest generation. Compressor power consumption

increases with ambient temperature (T_{amb}), peaking in August when temperatures are highest. During midday, abundant solar power meets the cooling demand efficiently, reducing battery reliance. However, after sunset, with zero solar output, the system depends fully on battery storage to power the compressor overnight, making battery capacity critical for continuous operation.

Figure 20 shows the battery configuration designed to store 825 Ah/day for nighttime compressor operation. This is achieved using seven 120 Ah batteries connected in parallel, ensuring uninterrupted power when solar energy is unavailable. The battery capacity is sized based on the peak August power consumption of 9 kWh/day—the highest summer demand—equivalent to 825 Ah/day. This sizing guarantees system reliability even during peak cooling loads. The number of batteries required was calculated using equation 19 from [17]:

$$\text{Number of Batteries} = \frac{825\text{Ah/day}}{120\text{ Ah/battery}} = 6.875 \text{ batteries} \approx 7 \text{ batteries} \quad (19)$$

Solar generation peaks in May, exceeding the compressor's consumption and allowing excess energy to charge the batteries for later use. In contrast, September has the lowest solar output, requiring more battery power to meet demand. The total charging current needed is 69 A, calculated by dividing the battery capacity by daylight hours, as per equation 20 [17]:

$$\text{Charging current} = \frac{825\text{ Ah/day}}{\text{daylight hours}} = \frac{825\text{Ah/day}}{12\text{ hours/day}} = 69\text{Amperes} \quad (20)$$

With a current of 10 Amperes per solar panel, the number of panels required is calculated as per equation 21[17]:

$$\text{Number of Panels} = \frac{69\text{ Amperes}}{10\text{ Amperes/panel}} = 6.9 \text{ panels} \approx 7\text{panels} \quad (21)$$

The system is designed with increased battery capacity to handle solar power fluctuations, ensuring the compressor always meets its power demand regardless of time or season. Battery capacity and solar panel count were sized based on August's peak power consumption, guaranteeing sufficient solar generation during the day. Batteries are charged when solar power is abundant and discharge at night, providing energy self-sufficiency and continuous operation. Overall, the system balances solar generation and battery storage to maintain efficiency and reliability, emphasizing the critical role of properly sized energy storage to meet seasonal variations in solar radiation and cooling demand.

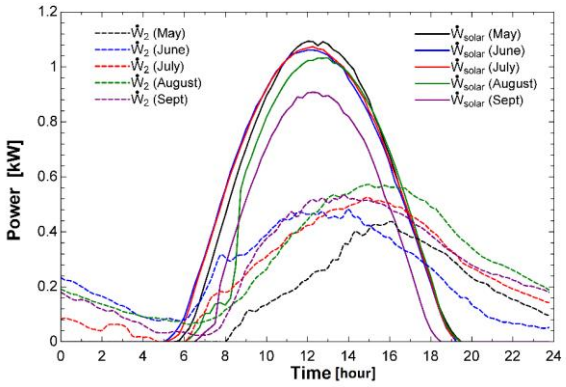

Figure 19. Solar power generation ($\dot{W}_{solar}$) and compressor power consumption ($\dot{W}_2$) as functions of time for representative average days across the summer months.

7.3. Effect of PV system area on compressor power consumption

Figure 21 illustrates the variation in compressor power consumption for different PV panel areas (2.8 m², 6.4 m², and 7.4 m²) during a typical day in August. The key observations from this analysis are:

1. **Influence of photovoltaic (PV) panel area on power output.** As the area of photovoltaic panels increases, an increased amount of solar energy is captured, resulting in increased electrical power output. The power output from the 7.4 m² panel is the most, succeeded by the 6.4 m² and 2.8 m². The power requirement of the compressor ($\dot{W}_2$) remains consistently steady throughout the day.
2. **Excess production and energy waste.** The photovoltaic system of 7.4 m² area generates surplus power, reaching a maximum of nearly 1.2 kW at midday. This greatly surpasses the compressor's requirements, resulting in energy wastage and superfluous system expenses.Thephotovoltaic system of 2.8 m²area generates insufficient electricity, failing to fully sustain the compressor's functioning.
3. **Panel size selection.** The PV panels of 6.4 m² produces sufficient energy to power the compressor effectively while minimizing surplus energy losses. This panel size optimizes cost efficiency and energy adequacy, rendering it the most appropriate choice for incorporation into the trans-critical CO_2 refrigeration system.

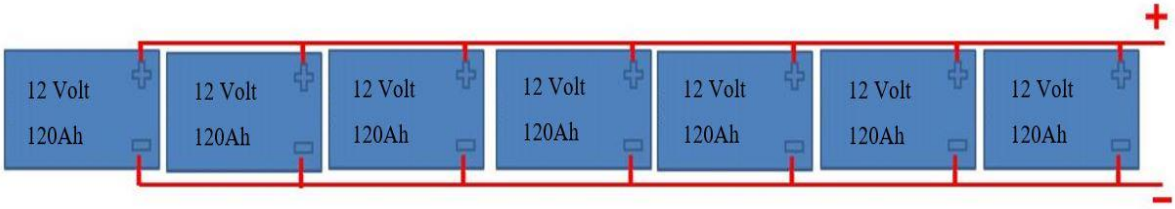

Figure 20. Batteries connection configuration

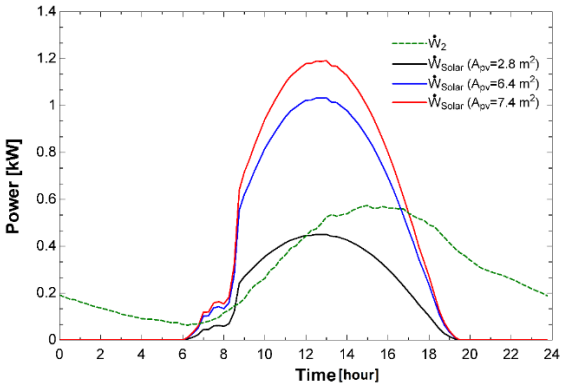

Figure 21. The power demand of the mechanical subcooling cycle on a representative average day in August for varying photovoltaic (PV) panel areas.

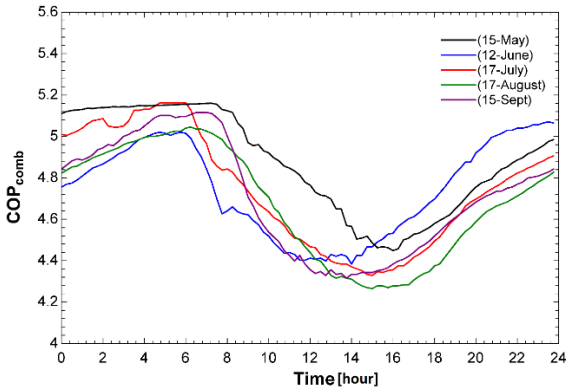

Figure22.COP_{comb}versus time for the average days of summer months

7.4. COP analysis of a solar-powered mechanical subcooling trans-critical CO_2 refrigeration system

The performance of the trans-critical CO_2 refrigeration system with solar-powered mechanical subcooling is highly affected by ambient temperature variations. **Figure 22** shows the hourly COP_{comb} across summer months, with efficiency dropping during hot midday hours and improving during cooler periods. From midnight to sunrise, low ambient temperatures reduce the heat load, allowing the compressor to operate efficiently with minimal power. Improved heat rejection from the gas cooler during these hours results in higher COP_{comb}. As morning temperatures rise, efficiency begins to decline due to increased compressor workload and reduced heat rejection capacity. The lowest COP_{comb} values occur in the early afternoon, particularly in August, where COP_{comb} drops to 4.3 at 16:00 PM, showing a 13% decline due to high thermal stress and increased power consumption. In contrast, May records the best performance, reaching COP_{comb} of 5.1 at 08:00 AM, with June, July, and September showing values between 4.2 and 5.0. To improve performance, cooling operations should be scheduled during early morning or evening. Thermal storage systems can store cooling capacity during high-COP periods, while optimized heat exchangers and advanced compressor controls can improve heat rejection and energy efficiency during hot hours. A 6.4 m² solar panel area is identified as the most cost-effective size, matching energy demand without overproduction or excess cost. Oversizing the PV system should be avoided to prevent energy waste.

In summary, COP_{comb} peaks in cooler periods and drops during heat extremes, with August showing the lowest efficiency and May the highest. Optimizing cooling schedules, integrating thermal storage, and selecting the right PV size are essential for enhancing efficiency and economic viability.

7.5. Energy savings analysis of a solar-powered mechanical subcooling system

The solar-powered mechanical subcooling system effectively reduces compressor energy consumption using solar PV, with energy savings varying by month. **Table IV** shows daily solar energy production, compressor consumption, and saved energy percentages. The highest solar output occurs in June (8.991 kWh), while the peak compressor energy use is in August (6.995 kWh). The highest energy savings are achieved in May (68.3%), due to moderate temperatures and ample solar energy. Savings in other months are 49.1% (June), 51.4% (July), 44.6% (August), and 37.7% (September). Despite high solar generation in June and July, rising cooling loads reduce overall savings. In August, nighttime compressor demand is highest (3.235 kWh), lowering efficiency. September's low solar output (6.451 kWh) and sustained cooling needs result in the lowest savings. These results confirm that solar-powered subcooling significantly reduces grid energy use, especially in May, and enhances efficiency during high-demand summer months.

Table IV. Total daily solar energy production, compressor energy consumption, and percentage of saved energy during daylight hours

Average day of month	Total daily energy produced from solar PV (kWh)	Energy required to the compressor of mechanical sub-cooling cycle during day light (kWh)	Energy required to the compressor of mechanical sub-cooling cycle during night (kWh)	Saved energy during day light (%)
15-May	8.745	2.416	1.473	68.3
12-June	8.991	4.273	1.567	49.1
17- July	8.919	3.884	2.079	51.4
17-August	7.905	3.760	3.235	44.6
15- Sept	6.451	3.479	2.973	37.7

7.6. Economic feasibility study for a 14 kW trans-critical CO_2 cycle with solar-powered mechanical sub-cooling in Jordan [30]

The main assumptions considered during this feasibility study are:

- Solar radiation in Jordan diminishes during winter, although remains capable of generating usable energy.
- The system functions with reduced sub-cooling loads outside of summer, resulting in decreased savings.
- Real-world discrepancies (e.g., efficiency losses) are disregarded for the sake of simplification.

The primary costs for implementing the solar-powered mechanical sub-cooling system in Jordan include (assumed as per the prices in Jordan) [31]:

- Solar PV system (6.4 m², 2 kW capacity) + installation: Around $3,000
- Mechanical sub-cooling system components (compressor, heat exchanger, control unit, R423A refrigerant): A round ($1000)
- Total initial investment cost: Around ($4000)

Jordan has an average daily solar radiation of 5.5–6.5 kWh/m²[25], making solar energy a viable option for reducing mechanical sub-cooling power consumption. Based on the total daily energy produced from solar PV in (kWh)found in **TableIV**, the energy saved per month can be found by multiplying the total monthly solar PVenergy (kWh) by the saved energy percentage for each month as shown in **Table V**.

Table V. Energy saved per month (kWh)

Month	Total Monthly Solar PV Energy (kWh)	Saved Energy (%)	Energy Saved (kWh)
May	8.745 × 30 = 262.35	68.3%	179.1
June	8.991 × 30 = 269.73	49.1%	132.4
July	8.919 × 30 = 267.57	51.4%	137.5
August	7.905 × 30 = 237.15	44.6%	105.8
Sept	6.451 × 30 = 193.53	37.7%	73.0
Summer energy savings	1,230.2 kWh		

Since the given data covers only five summer months (May–Sept), the annual savings is estimated by assuming that, savings during the remaining months (October–April) would be approximately 50% of the summer energy savings, due to reduced solar radiation[25].

- The annual energy saving in the months (October–April) can be estimated as: Summer energy savings× 50% = 1,230.2kWh×50% = 615.1 kWh
- Total annual energy savings: 1,230.2 kWh+615.1 kWh= 1845.3 kWh/year.
- Average electricity tariff in Jordan [30]: $0.10–$0.15/kWh (residential) and $0.17–$0.25/kWh (commercial/industrial).

The total annual financial savings can be calculated as per equation 22:

Annual financial savings =Total annual energy savings × Average electricity tariff in Jordan (22)

Annual financial savings for (commercial rate ($0.17/kWh))=1845.3 kWh/year ×$0.17/kWh= $313.70 /year

Annual financial savings for (residential rate ($0.12/kWh))= 1845.3 kWh/year ×$0.12 /kWh = $221.44 /year.

Annual financial savings for (Industrial rate ($0.226/kWh))= 1845.3 kWh/year ×$0.25/kWh= $417.08/year, which is the best-case scenario.

The payback period can be calculated according to equation 23[29]:

$$\text{payback period} = \frac{\text{Initial invetment}}{\text{Anual saving}} \quad (23)$$

Using equation 23,thepayback periods for different energy cost scenariosare summarized in Table**VI**:

Table VI. Payback periods for different energy cost scenarios

Scenario	Initial investment(USD)	Annual savings (USD)	Payback period
Industrial electricity rate ($0.25/kWh)	4000	417.03	9.6years
Commercial rate ($0.17/kWh)	4000	313.70	12.7 years
Residential rate ($0.12/kWh)	4000	221.44	18 years
With 30% government subsidy	2800	417.03	6.7years
With 50% government subsidy	2000	417.03	4.8years

This economic analysis assesses the payback period of the energy-saving system under various electricity tariffs and subsidy levels. As shown in **Table VI**, a $4000 initial investment results in payback periods of 9.6 years (industrial rate: $0.226/kWh), 12.7 years (commercial: $0.17/kWh), and 18 years (residential: $0.12/kWh).Government subsidies significantly improve feasibility. A 30% subsidy reduces the investment to $2800, shortening the payback to 6.7 years, while a 50% subsidy lowers it to $2000, with a 4.8-year payback.

In summary, the system is economically viable in Jordan, especially with subsidies. The shortest payback of 4.8 years occurs under industrial tariffs with a 50% subsidy, making the system most attractive for sectors with high energy costs and continuous operation.

8. Uncertainty analysis

An uncertainty analysis was conducted to evaluate the reliability of the simulated combined coefficient of performance (COP_{comb}) and combined power consumption ($\dot{W}_{comb}$). The analysis considered the key input parameters listed below, with assumed uncertainties based on standard engineering practice and literature.

The total uncertainty in the output was estimated using the Root Sum Square (RSS) method using equation 24:

$$U(f) = \sqrt{\left[\begin{matrix}(\partial f/\partial x_1 . \Delta x_1)^2 + (\partial f/\partial x_2 . \Delta x_2)^2 + \cdots \\ +(\partial f/\partial x_n . \Delta x_n)^2\end{matrix}\right]} \quad (24)$$

Where:

- f is the output function (e.g., COP_{comb} or $\dot{W}_{comb}$)
- x_n are the input parameters
- Δx_n are the assumed uncertainties for each input

The representative nominal values of $COP_{comb}$and $\dot{W}_{comb}$are 3 and 4.5 kW, respectively.

The assumed uncertainties of input parameters are shown in **Table VII.**

Table VII. Assumed Uncertainties of Input Parameters.

Parameter	Symbol	Nominal Value	Assumed Uncertainty
Evaporation temperature	T_{evap}	16 °C	±1.0 °C
Gas cooler outlet temperature	T_{gco}	45 °C	±1.0 °C
Gas cooler pressure	P_{gc}	10,000 kPa	±50 kPa
Subcooling temperature difference	ΔT_{sub}	10 °C	±1.0 °C
Superheat temperature difference	ΔT_{sup}	0 °C	±1.0 °C
Compressor efficiency	η_{comp}	0.80	±0.02

Based on equation 24 and the assumed uncertainties the Calculated Uncertainties in Output Parametersare shown in **Table VIII**.

Table VIII. Calculated uncertainties in output parameters

Output Parameter	Symbol	Value	Absolute Uncertainty	Relative Uncertainty (Absolute Uncertainty)/Value
Combined COP	COP_{comb}	3.0	±0.081	2.7%
Combined power consumption	$\dot{W}_{comb}$	4.5 kW	±0.134 kW	3.0%

The relative uncertainties in COP_{comb} and $\dot{W}_{comb}$ remain within 3%, as concluded from **Tables VII and VIII**, indicating a strong level of confidence in the simulation results. These uncertainties are based on realistic and commonly accepted input tolerances in thermodynamic modeling, ensuring a reliable assessment of the model's accuracy and predictive capability.

9. Conclusions

1. The integration of a mechanical sub-cooling cycle with a trans-critical CO_2 system significantly improved efficiency, achieving a 70.83% increase in COP_{comb}at high sub-cooling levels and 148% at optimized gas cooler pressure.
2. Sub-cooling optimization is critical: increasing it to 14°C raised compressor power by 70–80%, with a faster increase beyond 10°C. Superheat added 25–35% power consumption across all sub-cooling levels. While COP_{comb} improved by 70–75% at 14°C, excessive sub-cooling reduced gains by ~30%, highlighting the trade-off between efficiency and energy use.
3. Solar PV utilization yielded the highest energy savings in May (68.3%) and the lowest in September (37.7%), confirming system feasibility for summer operation.
4. An optimal 6.4 m² solar panel area was identified, balancing generation with compressor demand while minimizing excess energy and cost.
5. Simulation results closely matched experimental data, with 7.9% deviation in COP_{comb} and 4.35% in cooling capacity, validating model accuracy. The sub-cooling cycle also reduced P_{gc}, enhancing stability.
6. Economic analysis showed notable electricity cost reductions, with payback periods as low as 4.8 years (with subsidies), confirming cost-effectiveness for commercial and industrial use.
7. Overall, the system reliably delivered extra cooling in hot months while reducing grid dependence. Solar-powered sub-cooling proved a viable, sustainable strategy for enhancing trans-critical CO_2 system performance in high-temperature regions like Jordan.

References

[1] B. Dai, S. Liu, Z. Sun, and Y. Ma, "Thermodynamic performance analysis of CO_2 transcritical refrigeration cycle assisted with mechanical subcooling", *Energy Procedia*, vol. 105, pp. 2033–2038, 2017.https://doi.org/10.1016/j.egypro.2017.03.579.

[2] L. Nebot-Andrés, R. Llopis, D. Sánchez, J. Catalán-Gil, and R. Cabello, "CO_2 with mechanical subcooling vs. CO_2 cascade cycles for medium temperature commercial refrigeration applications thermodynamic analysis", *Applied Sciences*, vol. 7, no. 9, p. 955, 2017.https://doi.org/10.3390/app7090955.

[3] J. Catalán-Gil, R. Llopis, D. Sánchez, L. Nebot-Andres, and R. Cabello, "Energy analysis of dedicated and integrated mechanical subcooled CO_2 boosters for supermarket applications", *International Journal of Refrigeration*, vol. 101, pp. 11–23, 2019. https://doi.org/10.1016/j.ijrefrig.2019.01.034.

[4] R. Llopis, R. Cabello, D. Sánchez, and E. Torrella, "Energy improvements of CO_2 transcritical refrigeration cycles using dedicated mechanical subcooling", *International Journal of Refrigeration*, vol. 55, pp. 129–141, 2015.https://doi.org/10.1016/j.ijrefrig.2015.03.016.

[5] F. Cao, C. Cui, X. Wei, X. Yin, M. Li, and X. Wang, "The experimental investigation on a novel transcritical CO_2 heat pump combined system for space heating",*International Journal of Refrigeration*, vol. 106, pp. 539–548, 2019. https://doi.org/10.1016/j.ijrefrig.2019.05.004.

[6] A. M. Bahman, E. A. Groll, W. T. Horton, and J. E. Braun, "Technologies to improve the performance of A/C systems in hot climate regions", 15th International Refrigeration and Air Conditioning Conference, Purdue,United States of America, Paper 1431, 2014. http://docs.lib.purdue.edu/iracc/1431.

[7] A. Şencan, R. Selbaş, Ö. Kızılkan, and S. A. Kalogirou, "Thermodynamic analysis of subcooling and superheating effects of alternative refrigerants for vapour compression refrigeration cycles", *International Journal of Energy Research*, vol. 30, no. 5, pp. 323–347, 2006. https://doi.org/10.1002/er.1151.

[8] X. R. Zhang, H. Yamaguchi, K. Fujima, M. Enomoto, and N. Sawada, "Study of solar energy powered transcritical cycle using supercritical carbon dioxide", *International Journal of Energy Research*, vol. 30, no. 14, pp. 1117–1129, 2006. https://doi.org/10.1002/er.1201.

[9] A. Farraj, M. Abu Mallouh, A.-R. Kalendar, and A. Al-Rzaq, "Experimental study of solar powered air conditioning unit using drop–in hydrocarbon mixture to replace R-22", *Jordan Journal of Mechanical and Industrial Engineering (JJMIE)*, vol. 6, no. 1, pp. 63-70, 2012.https://jjmie.hu.edu.jo/files/v6n1/JIMIE-171-10.pdf.

[10] A. M. Jawarneh, M.Al-Tarawneh, M. K. Ababneh, and H. Tlilan, "Solar energy availability on horizontal and tilted surfaces: A case study" *International Review of Mechanical Engineering*, vol. 6, no. 4, pp. 901–917, 2012.

[11] Z. Li, E. Chen, Y. Jing, and S. Lv, "Thermodynamic relationship of subcooling power and increase of cooling output in vapour compression chiller", *Energy Conversion and Management*, vol. 149, pp. 254–262, 2017.https://doi.org/10.1016/j.enconman.2017.07.030.

[12] M. Zeyghami, D. Y. Goswami, and E. Stefanakos, "A review of solar thermo-mechanical refrigeration and cooling methods", *Renewable and Sustainable Energy Reviews*, vol. 51, pp. 1428–1445, 2015.https://doi.org/10.1016/j.rser.2015.07.011.

[13] I. Sarbu and C. Sebarchievici, "Review of solar refrigeration and cooling systems", *Energy and Buildings*, vol. 67, pp. 286–297, 2013. https://doi.org/10.1016/j.enbuild.2013.08.022.

[14] E. Bellos, M. G. Vrachopoulos, and C. Tzivanidis, "Energetic and exergetic investigation of a novel solar assisted mechanical compression refrigeration system", *Energy Conversion and Management*, vol. 147, pp. 1–18, 2017. https://doi.org/10.1016/j.enconman.2017.05.040.

[15] F. Hanslik, J. Suess, and J. Koehler, "Efficiency enhancement by subcooling the carbon dioxide process with water as refrigerant," 17th International Refrigeration and Air Conditioning Conference, Purdue,United States of America, Paper 1855, 2018. https://docs.lib.purdue.edu/cgi/viewcontent. =cgi?article=2854&context=iracc.

[16] I. D. M. C. Santosa, I. G. N. S. Waisnawa, P. W. Sunu, and I. W. Temaja, "Simulation of transcritical CO_2 refrigeration system with booster hot gas bypass in tropical climate", *Journal of Physics: Conference Series*, vol. 953, no. 1, p. 012044, IOP Publishing, 2018.https://doi.org/10.1088/1742-6596/953/1/012044.

[17] S. Barghash, A. Bahman, and O. Ibrahim, "Solar-powered mechanical subcooling refrigeration system for hot climates", 18th International Refrigeration and Air Conditioning Conference, Purdue,United States of America, Paper 2129, 2021.https://docs.lib.purdue.edu/cgi/viewcontent.cgi?article=3128&context=iracc.

[18] Mohammad Tarawneh, "Effect of using a porous gas cooler on the performance of trans-critical carbon dioxide refrigeration cycle," *Heat Transfer*, vol. 51, no. 2, pp. 2306–2317, 2022. https://doi.org/10.1002/htj.22401.

[19] Mohammad Tarawneh, "Performance enhancement of a split air conditioner using porous material inside the evaporator pipes", *Heat Transfer*, vol. 51, no. 2, pp. 2114–2128, 2022.https://doi.org/10.1002/htj.22391.

[20] Mohammad Tarawneh, A. M. Jawarneh, H. Tlilan, A. Ababneh, and A. Al–Migdady, "Investigation of the effect of superheating on the performance of a refrigeration system using low temperature different refrigerant blends in porous media", *Heat Transfer-Asian Research*, vol. 48, no. 6, pp. 2216–2236, 2019.https://doi.org/10.1002/htj.21481.

[21] R. Llopis, L. Nebot-Andrés, R. Cabello, D. Sánchez, and J. Catalán-Gil, "Experimental evaluation of a CO_2 transcritical refrigeration plant with dedicated mechanical subcooling", *International Journal of Refrigeration*, vol. 69, pp. 361–368, 2016. https://doi.org/10.1016/j.ijrefrig.2016.06.009.

[22] A. Guedour, A. Bahman, and O. Ibrahim, "Exergy, environmental, and economic analyses of solar-powered dedicated mechanical subcooling refrigeration in hot climates", 20th International Refrigeration and Air Conditioning Conference, Purdue,United States of America, Paper 2593, 2024. https://docs.lib.purdue.edu/cgi/viewcontent.cgi?article=3592&context=iracc.

[23] Mohammad Tarawneh and E. B. Melhem, "Hybrid solar-assisted trans-critical CO_2 refrigeration cycle optimization with internal heat exchange for hot climate applications", *Thermal Science and Engineering Progress*, vol. 60, p. 103492, 2025. https://doi.org/10.1016/j.tsep.2025.103492.

[24] X. Qin, S. Lei, H. Liu, Y. Zeng, Y. Liu, C. Pang, and J. Chen, "Comparative analysis of transcritical CO_2 heat pump systems with and without ejector: Performance, exergy, and economic perspective," *Energies*, vol. 18, no. 12, p. 3223, 2025.https://doi.org/10.3390/en18123223.

[25] Ministry of Energy and Mineral Resources (MEMR), Annual Reports, Amman, Jordan, 2023.https://www.memr.gov.jo/ebv4.0/root_storage/en/eb_list_page/annual_report_20233.pdf.

[26] M.-H. Kim, J. Pettersen, and C. W. Bullard, "Fundamental process and system design issues in CO_2 vapor compression systems", *Progress in Energy and Combustion Science*, vol. 30, no. 2, pp. 119–174, 2004. https://doi.org/10.1016/j.pecs.2003.09.002.

[27] S. Kurtz, K. Whitfield, G. TamizhMani, M. Koehl, D. Miller, J. Joyce, J. Wohlgemuth, N. Bosco, M. Kempe, and T. Zgonena, "Evaluation of high-temperature exposure of photovoltaic modules," *Progress in Photovoltaics: Research and Applications*, vol. 19, no. 8, pp. 954–965, 2011. https://doi.org/10.1002/pip.1103.

[28] S. A. Klein, *Engineering Equation Solver Academic Commercial V9*, F-Chart Software, LLC. Madison, WI.2015. https://fchartsoftware.com/ees/.

[29] L. Wang, Y. Zhang, and G. Ma, "Theoretical investigation of a novel distributed compression cycle for CO_2 trans-critical system", *Energy and Buildings*, vol. 304, p. 113853, 2024.https://doi.org/10.1016/j.enbuild.2023.113853.

[30] A. Teke, O. Timur, and K. Zor, "Calculating payback periods for energy efficiency improvement applications at a university hospital",*Çukurova University Journal of the Faculty of Engineering and Architecture*, vol. 30, no. 1, pp. 41–56, 2015. https://dergipark.org.tr/tr/download/article-file/211206.

[31] Jordan Energy and Minerals Regulatory Commission (JEMRC). 2024. https://www.nepco.com.jo/assets/doc/ tariff. pdf.